INSTITUTE OF PHYSICS PUBLISHING PHYSICS IN MEDICINE AND BIOLOGY

Phys. Med. Biol. **47** (2002) 1837–1851 PII: S0031-9155(02)34700-6

Experimental validation of the DPM Monte Carlo code using minimally scattered electron beams in heterogeneous media

Indrin J Chetty[1], **Jean M Moran**[1], **Teamor S Nurushev**[1], **Daniel L McShan**[1], **Benedick A Fraass**[1], **Scott J Wilderman**[2] **and Alex F Bielajew**[2]

[1] Department of Radiation Oncology, The University of Michigan, Ann Arbor, MI 48109-0010, USA
[2] Department of Nuclear Engineering, The University of Michigan, Ann Arbor, MI 48109-2104, USA

E-mail: indrin@med.umich.edu

Received 11 March 2002
Published 22 May 2002
Online at stacks.iop.org/PMB/47/1837

Abstract

A comprehensive set of measurements and calculations has been conducted to investigate the accuracy of the Dose Planning Method (DPM) Monte Carlo code for electron beam dose calculations in heterogeneous media. Measurements were made using 10 MeV and 50 MeV minimally scattered, uncollimated electron beams from a racetrack microtron. Source distributions for the Monte Carlo calculations were reconstructed from in-air ion chamber scans and then benchmarked against measurements in a homogeneous water phantom. The in-air spatial distributions were found to have FWHM of 4.7 cm and 1.3 cm, at 100 cm from the source, for the 10 MeV and 50 MeV beams respectively. Energy spectra for the electron beams were determined by simulating the components of the microtron treatment head using the code MCNP4B. Profile measurements were made using an ion chamber in a water phantom with slabs of lung or bone-equivalent materials submerged at various depths. DPM calculations are, on average, within 2% agreement with measurement for all geometries except for the 50 MeV incident on a 6 cm lung-equivalent slab. Measurements using approximately monoenergetic, 50 MeV, 'pencil-beam'-type electrons in heterogeneous media provide conditions for maximum electronic disequilibrium and hence present a stringent test of the code's electron transport physics; the agreement noted between calculation and measurement illustrates that the DPM code is capable of accurate dose calculation even under such conditions.

 © 2002 IOP Publishing Ltd Printed in the UK

1. Introduction

The application of the Monte Carlo method to the study of linear accelerators and radiotherapy dose calculations has been steadily increasing over recent years. Much effort has been devoted to testing and modifying Monte Carlo codes for research-related dosimetry studies as well as for use in clinical radiotherapy treatment planning (DeMarco *et al* 1998, Wang *et al* 1998, Ma *et al* 1999, Sempau *et al* 2000, 2001, Kawrakow and Fippel 2000, Schach von Wittenau *et al* 1999, Fix *et al* 2001, Keall *et al* 2001). Despite the rapid evolution of Monte Carlo methods for radiotherapy dose calculations, the use of this method for routine clinical radiotherapy planning within a reasonable amount of time still remains a concern (Lovelock *et al* 1995, Rogers *et al* 1995). The limitation in processing times for Monte Carlo dose calculations has prompted researchers to improve the efficiency of their Monte Carlo dose engines. Two examples of this are the MCDOSE and XVMC codes developed by Ma *et al* (2000) and Kawrakow and Fippel (2000) respectively. Both these codes make use of a variety of variance reduction techniques, including photon forcing, Russian roulette and electron track repeating, in order to improve the dose calculation efficiency.

A new Monte Carlo code, the Dose Planning Method (DPM), which is the focus of this work, has been developed by Sempau *et al* (2000). DPM employs several features that make it optimal for radiotherapy class dose calculations. These include: (a) the use of a step-size independent multiple scattering theory, (b) the use of a 'random hinge' scheme in transporting charged particles from point-to-point in the medium, (c) the use of large electron steps which affords the ability to traverse many voxels before sampling a multiple scattering angle, and (d) the use of woodcock tracking to reduce the overheads associated with transporting photons across boundaries. Details of the electron/photon transport model used in DPM along with accuracy and efficiency comparisons are provided by Sempau *et al* (2000).

In this current work we have benchmarked the DPM code against measurements in heterogeneous media using minimally scattered, uncollimated electron beams produced from a racetrack microtron. Although Sempau *et al* (2000) established the accuracy of DPM relative to other well-established Monte Carlo codes, such as EGS4/Presta, Penelope and MCNP, no experimental validation was provided in their study. Extension of the work by Sempau *et al* (2000) for dose calculations in a clinical setting requires testing of the code against standard measurements in a water phantom. The motivation for this work was to conduct experiments that would provide a stringent test of the transport physics used in the code; the lateral disequilibrium observed with high-energy, monoenergetic, pencil-beam electrons in heterogeneous media, for example, poses a challenging test of the physics for any dose computational algorithm. The 50 MeV electron beam used in this study was approximately monoenergetic, with a pencil-beam-type spatial distribution (FWHM of 1.3 cm at 100 cm from the source). The monoenergetic, pencil beam nature of the 50 MeV electron beam meant that DPM calculations could be conducted with minimal source-modelling requirement. The resulting lateral electronic disequilibrium observed with 50 MeV electrons at inhomogeneous interfaces was found to be ideal for evaluating the transport physics used in DPM.

The scope of this paper includes the following areas: Monte Carlo simulation of the racetrack microtron treatment head for 10 MeV and 50 MeV electron beams, the experimental set-up, the Monte Carlo source description and scoring parameters, and finally, dose comparisons between measurements and calculations in both homogeneous- and inhomogeneous-type geometries.

Table 1. Description of the treatment head of the Scanditronix Racetrack Microtron (Scanditronix, Uppsala, Sweden) for the 10 and 50 MeV uncollimated electron beams. Shown are the component composite materials, and the corresponding density-weighted thicknesses in g cm^{-2}. The data presented here are based on information provided by Scanditronix engineers. Simulation of the various components was conducted using the Monte Carlo method to determine the electron energy spectra.

Component	Material	Density-weighted thickness (g cm^{-2})
Entrance window	Beryllium	4.63×10^{-2}
Ion chamber	Layers of gold and polyamide (CH_2)	0.103
Mirror	Kapton	1.70×10^{-3}
Exit window	Mylar	2.40×10^{-3}
Medium within treatment head	Helium	7.70×10^{-3}
		Total = 0.161

2. Methods and materials

2.1. Monte Carlo simulation of the racetrack microtron treatment head

The Scanditronix racetrack microtron (Scanditronix, Uppsala, Sweden) was chosen for this study due to its simple treatment head design, the ability to deliver electron beams without scattering foils or beam collimators, and the range of energies up to 50 MeV (Brahme *et al* 1980, Gudowska *et al* 1999, Karlsson *et al* 1992, Liu *et al* 1995). The treatment head components along with their composite material types and density-weighted thicknesses are presented in table 1. Information in this table is based upon the information provided by Scanditronix engineers. The entire component thickness is approximately 0.2 g cm^{-2}, which minimizes energy losses and scattering in the treatment head. In addition, the entire treatment head, from the vacuum window to the exit window, is filled with helium. Karlsson *et al* (1992), in their paper on electron beam characteristics of the 50 MeV racetrack microtron, point out that the 80%–20% penumbra is reduced by a factor of two when the air-filled treatment head is replaced with helium; this is due to the much lower linear scattering power in helium. The modified treatment head design results in a 50 MeV beam that is nearly monoenergetic, and has a significantly smaller angular electron spread relative to other accelerators (Karlsson *et al* 1992).

The energy spectra of the 10 MeV and 50 MeV electron beams were calculated by Monte Carlo simulation of the treatment head components using the code MCNP4B (Briesmeister 2000). The scoring geometry consisted of a scoring slab intersected by concentric cylinders to produce annular rings, each having a radial width of 2 mm and an axial thickness of 2 mm. The total scoring radius extended to a distance of 7 cm outward from the central axis. The source was located at zero radius, 100 cm upstream from the scoring volumes. The MCNP F4 tally was used to score the energy fluence. The F4 tally uses a track length estimate of the particle fluence based on the track length of each particle through the cell volume (Briesmeister 2000). The F4 tally was chosen since it has been found to be a reliable estimate of fluence given that there are many tracks in a cell and hence many contributions to this tally (Briesmeister 2000). To obtain the incident electron, a trial and error method was used whereby each spectral distribution was calibrated against the corresponding central axis depth dose curve. This procedure involved calculating the energy fluence at the scoring plane from the treatment head simulation starting with an initial, monoenergetic, electron beam incident

at the beryllium entrance window. The scored energy fluence was subsequently sampled to calculate the depth dose in water; a comparison of the measured and calculated depth doses was performed to validate the choice of the initial electron beam energy. For the 50 MeV beam, it was found that starting with the 50 MeV monoenergetic electrons at the entrance window produced a nearly monoenergetic (50.0 MeV) electron fluence at the scoring plane (see figure 2(b), which when sampled to calculate the dose in water, was found to produce a depth dose curve in good agreement with measurements (see figure 3). For the 10 MeV beam, however, starting with monoenergetic 10 MeV electrons at the entrance window produced a depth dose curve that was less penetrating than that measured. As a result, the initial electron energy was further increased until the calculated depth dose was in good agreement ($\pm 2\%$) with the measurements—this initial energy was found to be 10.65 MeV. The process of 'calibrating' the incident electron energy is typically used for the Monte Carlo-based treatment head simulation, and has been previously described by other investigators (DeMarco *et al* 1998, Lovelock *et al* 1995, Rogers *et al* 1995). Unless the electron incident energy is accurately known *a priori*, the trial and error method provides the best means of determining the incident electron energy for use in the Monte Carlo treatment head simulation.

2.2. Experimental set-up and ion chamber measurements

In the experiments, the ion chamber measurements were acquired in air as well as within a water phantom of $40 \times 40 \times 40$ cm^3 dimensions. All measurements were conducted using a Scanditronix Type RK 83-05 ion chamber with an air-cavity volume of 0.12 cm^3 and a 2 mm inner radius. Central axis and off-axes 'in-air' transverse profile (x-axis) scans were taken for the 10 MeV beam, extending from -6.4 cm to 6.4 cm in the x-axis, and spanning a region from -6.4 cm to 6.4 cm in the y-axis in 2 mm increments. Transverse 'in-air' scans were acquired for the 50 MeV beam extending from -2.4 cm to 2.4 cm in the x-axis, and spanning a region from -2.4 cm to 2.4 cm in the y-axis in 2 mm increments. The central axis depth dose and profiles were measured at 100 cm SSD within the homogeneous water phantom. Profile scans were acquired along the central axis (along the transverse, x-axis) at the $d_{\max}$ depth, as well as the 90%, 50%, and 20% isodose regions.

Inhomogeneity measurements were conducted using lung and bone-equivalent slabs, with dimensions, 20 cm $\times$ 20 cm, and ranging in thickness from 2 cm to 6 cm. The mass densities of the lung and bone materials were 0.31 g cm^{-3} and 1.80 g cm^{-3} respectively. The slabs were submerged at various depths in the water and positioned in the half-slab-type geometry as illustrated in figure 1. Transverse (x-axis) profile scans were acquired, with the centre of the ion chamber positioned approximately 4 mm directly beneath the inhomogeneity, in order to assess the lateral electron disequilibrium at the slab/water interface.

For all ion chamber measurements in this work, relative ionization has been converted to relative dose by multiplying the relative ionization values by the restricted stopping power ratios, $(L/\rho)_{\text{air}}^{\text{water}}$, at the respective electron energy. Monte Carlo simulation (MCNP) was used to calculate the mean electron energies, averaged over each scoring voxel, for a given geometry set-up—this simulation was approximate in that it did not include the perturbation effects of the ion chamber. Stopping power ratios were extracted from the National Institutes of Standards and Technology (NIST) stopping power and range tables web-based database, compiled by Berger (1993).

2.3. Monte Carlo source description and scoring parameters

The Monte Carlo source description requires specification of the position, energy and angle for each starting particle. A 2D source spatial distribution was reconstructed from the 'in-air'

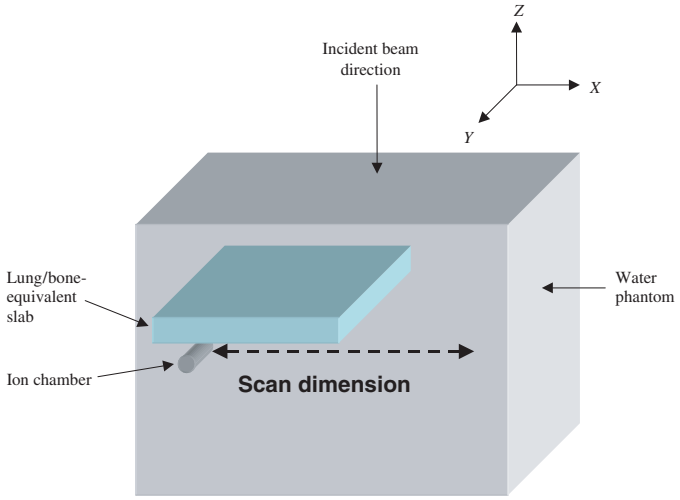

Figure 1. Experimental set-up for the heterogeneous profile measurements. The lung/bone equivalent slabs have dimensions of 20 × 20 cm^2 with varying thicknesses (2 cm–6 cm), and were positioned at various depths below the water surface along the negative *x*-axis of the tank. Profile scans were conducted with the centre of the ion chamber approximately 4 mm directly beneath the inhomogeneity.

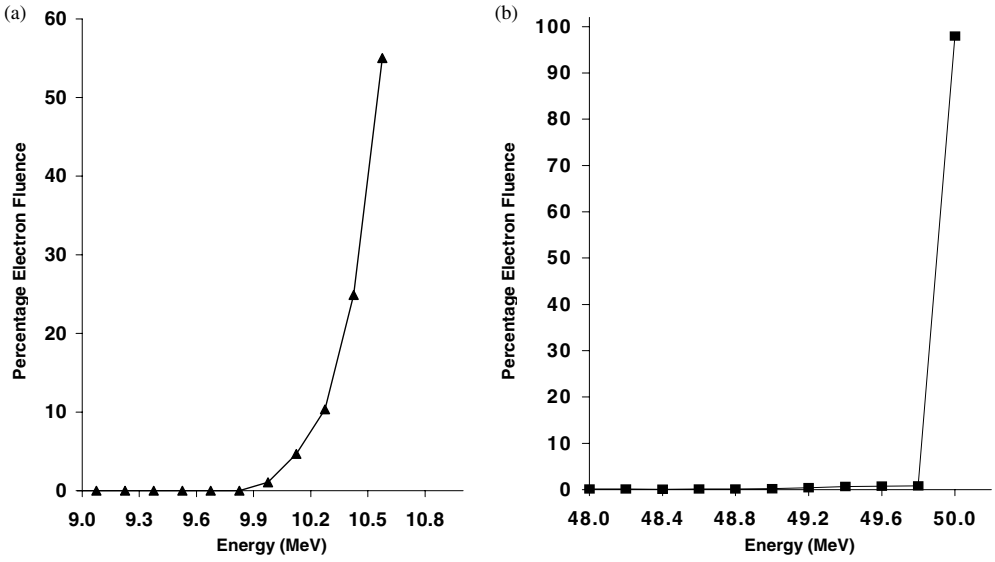

Figure 2. Percentage electron fluence as a function of energy for the 10 MeV (a) and the 50 MeV (b) electron beams from the MCNP Monte Carlo treatment head simulation of the racetrack microtron. The simulation was conducted starting with monoenergetic electrons of energies 10.65 MeV and 50.0 MeV for the 10 MeV and 50 MeV beams respectively. The electron fluence is averaged over the concentric cylinders extending from the central axis to a radial distance of 6 cm (50 MeV) and 4 cm (10 MeV). For the 10 MeV electron beam (a), 97% of the electrons occupy energies in the range from 9.9 MeV to 10.65 MeV, and 3% of the electrons reside in energy bins from 0 to 9 MeV (not shown on plot). For the 50 MeV beam (b), the majority of the electrons (98%) occupy energies in the range from 49.8 MeV to 50.0 MeV. A small percentage, 2%, of electrons reside in energy bins from 0 to 49.8 MeV.

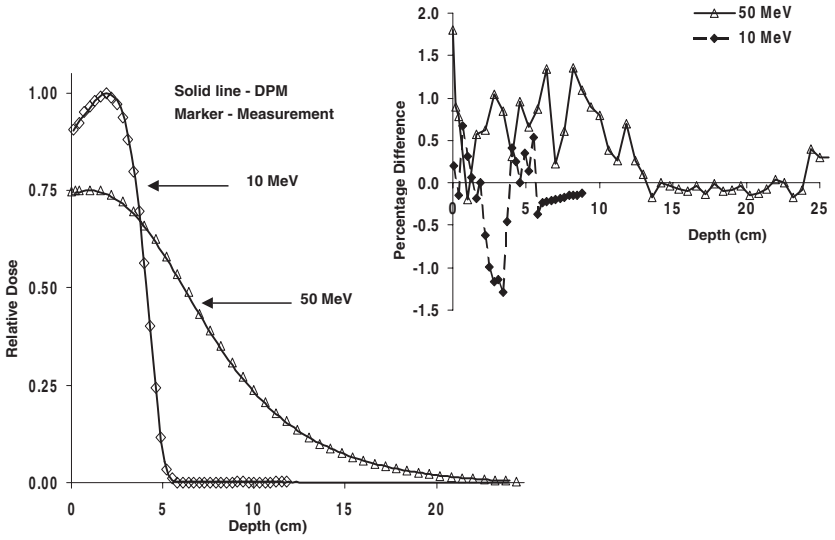

Figure 3. The 10 MeV and 50 MeV central axis depth dose comparison in the homogeneous water phantom. Measurements are shown with markers, and DPM in the solid line. Both curves are normalized to d_{max}. The 50 MeV plot is scaled by a factor of 0.75 for ease of illustration. The DPM calculated points represent the centre of voxel values. The 1σ Monte Carlo uncertainty averaged over all calculation points is 0.5%. Per cent differences between calculations and measurements for the depth dose comparisons are presented in the inset. Average differences are 0.3% (10 MeV) and 0.4% (50 MeV). For the 10 MeV profile, the 1σ Monte Carlo uncertainty ranged from 0.3% in the region of maximum dose to 0.4% in the region less than 10% of maximum dose. The respective 1σ uncertainty range for the 50 MeV profile was from 0.1% to 1.0%.

profile measurements for sampling the source particle's position within the DPM simulation. The radial fluence distribution was extracted from the measured transverse profiles—acquiring these scans in 2 mm increments allowed reconstruction of a finely sampled fluence matrix. For the 50 MeV beam, a monoenergetic 50.0 MeV electron source was used, while for the 10 MeV beam the electron's energy distribution (calculated using the MCNP F4 tally) was sampled as a function of the position within the scoring plane. The source particle's angle was calculated using a point source ($1/R^2$) divergence. Based on the agreement with the measurements (see results), the point source approximation provides an adequate description of the electron beam angular spread.

Calculations of dose using the DPM Monte Carlo code were performed using a simulated cubic water phantom with a side of 40 cm. A scoring voxel with dimensions 2 mm × 2 mm × 2 mm was used for all calculations. The low-energy electron and photon cut-offs were 200 keV and 50 keV respectively and the DPM step size was set at 2 mm for both 10 MeV and 50 MeV comparisons.

2.4. Profile normalization

Measured and calculation profiles have been normalized to the area under the respective curves. This method of normalization provides a fair means of comparison between calculations and measurements as the area under the curve represents the total energy deposited. If the Monte Carlo transport physics is correct, i.e. follows the conservation of energy, then the area under the curves for both calculations and measurements will be the same.

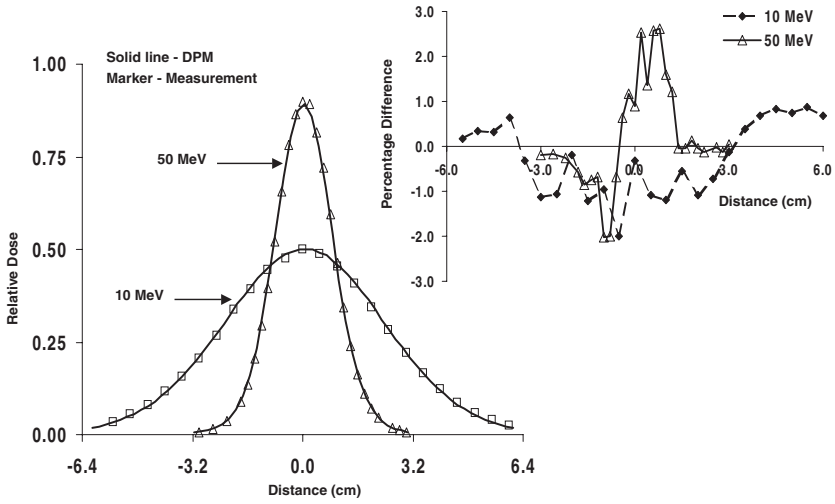

Figure 4. Central axis profile comparisons at the 50% isodose region for the 10 MeV and 50 MeV electron beams in the homogeneous water phantom. The 50% isodose region corresponds to the depths of 4.3 cm and 7.6 cm for the 10 MeV and 50 MeV beams respectively. Measurements are shown in the marker and DPM in the solid line. DPM calculated points represent the centre of voxel values. Profiles for each energy are normalized to the area under the corresponding curve. The 10 MeV comparison also includes an additional scaling factor (0.5) for ease of illustration. The 1σ Monte Carlo uncertainty averaged over all calculation points is 0.9% and 0.5% for the 10 MeV and 50 MeV electron beams respectively. Per cent differences between the calculations and measurements for the profile comparison at the 50% isodose region are illustrated in the inset. The average difference between measurements and calculations is 0.9% for both 10 MeV and 50 MeV profiles. For the 10 MeV profile, the 1σ Monte Carlo uncertainty ranged from 0.5% in the region of maximum dose to 1.8% in the region less than 10% of maximum dose. The respective 1σ uncertainty range for the 50 MeV profile was from 0.2% to 1.7%.

3. Results and discussion

3.1. Homogeneous phantom

Figure 2 illustrates the percentage electron fluence averaged over the scoring plane as a function of energy for the 10 MeV (figure 2(a)) and 50 MeV (figure 2(b)) electron beams respectively. Each energy bin in figure 2(a) has a width of 0.15 MeV. It is noted that 96% of the electron fluence is accounted for in the energy region from 9.9 MeV to 10.65 MeV. Although not explicitly illustrated on the plot, simulation results indicate that approximately 3% of the electrons have energies in the range from 0 to 9 MeV. From figure 2(b) it is seen that 98% of electrons have energies in the range from 49.8 MeV to 50.0 MeV; each bin here has a width of 0.2 MeV. The remaining 2% of the electrons occupy energies in the region from 0 to 49.8 MeV. These results suggest that the energy losses due to scattering in the microtron treatment head are minimal for the 50 MeV beam.

Figure 3 illustrates the central axis depth dose curves for the 10 MeV and 50 MeV uncollimated electron beams respectively, normalized to the maximum dose. The 50 MeV depth dose plot includes a scaling factor of 0.75 for ease of illustration. Plots of the per cent differences between DPM and measurements as well as the 1σ Monte Carlo statistical uncertainty are shown in the inset. The average differences between measurements and DPM are 0.3% and 0.4% for the 10 MeV and 50 MeV electron beams respectively; these average differences are well within the 2% agreement with measurements. Figure 4 represents

Table 2. Experimental set-up and calculation details for the inhomogeneous profile comparisons. Specifically shown are the electron beam energy, the type and position (in cm) of the inhomogeneity within the water tank, the depth of the profile measurement and scoring plane, the average and maximum per cent differences (in parentheses) between profile measurements and calculations, and the 1σ Monte Carlo uncertainty averaged over all calculation points. The water tank dimensions, in cm, are: $-20 \leqslant x \leqslant 20$, $-20 \leqslant y \leqslant 20$, $0 \leqslant z \leqslant 40$. The beam is incident from the location $x = 0$, $y = 0$, $z = 0$, where $z = 0$ corresponds to the top surface of the water phantom.

Fig no	Electron energy (MeV)	Description and position of the inhomogeneity within the water tank	Measurement/ scoring plane	Average % difference vs measurement (max diff)	Average % DPM uncertainty (1σ)
5	10	Bone-equivalent slab $-20 \leqslant x \leqslant 0$, $-10 \leqslant y \leqslant 10$, $0.5 \leqslant z \leqslant 2.5$	x-axis profile $-8 \leqslant x \leqslant 8$, $y = 0$ $z = 2.9$	1.9 (3.1)	1.0
5 (scaled)	10	Bone-equivalent slab $-20 \leqslant x \leqslant 0$, $-10 \leqslant y \leqslant 10$, $1.5 \leqslant z \leqslant 3.5$	x-axis profile $-8 \leqslant x \leqslant 8$, $y = 0$ $z = 3.9$	1.7 (3.2)	1.1
6	50	Bone-equivalent slab $-20 \leqslant x \leqslant 0$, $-10 \leqslant y \leqslant 10$, $1.5 \leqslant z \leqslant 5.5$	x-axis profile $-5 \leqslant x \leqslant 5$, $y = 0$ $z = 5.9$	0.8 (−2.9)	1.8
6 (scaled)	50	Bone-equivalent slab $-20 \leqslant x \leqslant 0$, $-10 \leqslant y \leqslant 10$, $3.0 \leqslant z \leqslant 7.0$	x-axis profile $-5 \leqslant x \leqslant 5$, $y = 0$ $z = 7.4$	1.1 (3.3)	1.2
7	10	Lung-equivalent slab $-20 \leqslant x \leqslant 0$, $-10 \leqslant y \leqslant 10$, $1.5 \leqslant z \leqslant 3.5$	x-axis profile $-8 \leqslant x \leqslant 8$, $y = 0$ $z = 3.9$	1.3 (−3.2)	1.0
7 (scaled)	10	Lung-equivalent slab $-20 \leqslant x \leqslant 0$, $-10 \leqslant y \leqslant 10$, $3.0 \leqslant z \leqslant 5.0$	x-axis profile $-8 \leqslant x \leqslant 8$, $y = 0$ $z = 5.4$	0.9 (−2.8)	0.9
8	10	Lung-equivalent slab $-20 \leqslant x \leqslant 0$, $-10 \leqslant y \leqslant 10$, $1.5 \leqslant z \leqslant 5.5$	x-axis profile $-8 \leqslant x \leqslant 8$, $y = 0$ $z = 5.9$	1.0 (−3.3)	1.0
8 (scaled)	10	Lung-equivalent slab $-20 \leqslant x \leqslant 0$, $-10 \leqslant y \leqslant 10$, $3.0 \leqslant z \leqslant 7.0$	x-axis profile $-8 \leqslant x \leqslant 8$, $y = 0$ $z = 7.4$	1.1 (3.3)	1.2
9	50	Lung-equivalent slab $-20 \leqslant x \leqslant 0$, $-10 \leqslant y \leqslant 10$, $1.5 \leqslant z \leqslant 7.5$	x-axis profile $-5 \leqslant x \leqslant 5$, $y = 0$ $z = 7.9$	7.8 (−16.6)	1.2
9 (scaled)	50	Lung-equivalent slab $-20 \leqslant x \leqslant 0$, $-10 \leqslant y \leqslant 10$, $4.5 \leqslant z \leqslant 10.5$	x-axis profile $-5 \leqslant x \leqslant 5$, $y = 0$ $z = 10.9$	4.9 (11.2)	1.1

the relative profile dose comparisons for the 10 MeV and 50 MeV beams at the 50% isodose region. The 50% isodose region corresponds to respective depths of 4.3 cm for the 10 MeV beam and 7.6 cm for the 50 MeV beam. The profile is normalized to the area under the curve. This figure illustrates the pencil beam nature of the 50 MeV beam; the FWHM of this profile (at depth of 7.6 cm) is 1.75 cm. The 10 MeV profile resembles a broad-beam, rather than a pencil-beam-type distribution, owing to the increased angular scattering and energy degradation for 10 MeV electrons. Percentage differences between DPM and measurements are illustrated in the inset. The difference plots were calculated as follows: (measured value − calculated value) × 100/maximum normalized measured value. The ±2%–±3% differences noted in the profiles are likely due to a combination of measurement uncertainty as well

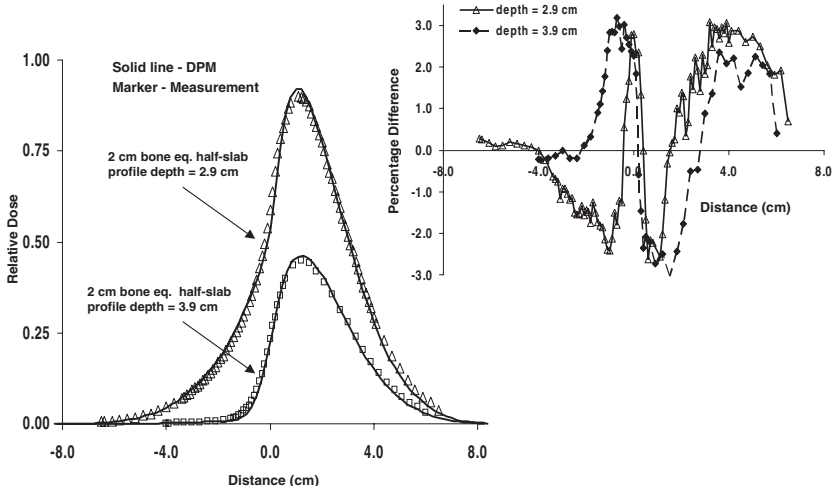

Figure 5. Relative x-axis profile dose for 10 MeV electrons incident on a 2 cm bone-equivalent half-slab positioned at depths of 0.5 cm and 1.5 cm below the water surface. Details of the geometric set-up are provided in table 2. Measurements are shown in the marker and the DPM in the solid line. Profiles are normalized to the area under the corresponding curve. The profile for the slab positioned at a depth of 1.5 cm below the water surface includes a scaling factor of 0.5 for ease of illustration. DPM calculated points represent the centre of the voxel values. The 1σ Monte Carlo uncertainty averaged over all calculation points is 1.0% for the slab located at 0.5 cm depth, and 1.1% for the slab at 1.5 cm depth below the water surface. Per cent differences between calculations and measurements illustrated for the corresponding profiles in the inset. Average and maximum differences between the measurements and calculations are provided in table 2. The 1σ Monte Carlo uncertainty ranged from 0.5% in the region of the maximum profile dose to 2.8% in the region less than 10% of maximum dose, for the slab positioned at 0.5 cm depth below the water surface. The corresponding 1σ uncertainty range for the slab at a depth of 1.5 cm was 0.5% to 2.4%.

as errors caused by interpolation during reconstruction of the fluence map from in-air fluence measurements (Chetty *et al* 2002). A detailed analysis of 10 MeV and 50 MeV DPM calculations versus measurements in homogeneous situations is presented by Chetty *et al* (2002).

3.2. Inhomogeneous phantom

Profile comparisons for the inhomogeneous-type geometries are illustrated in figures 5–9; per cent differences between measurements and calculations are presented in the insets for these corresponding profiles. All inhomogeneous comparisons in this study are conducted using the 'half-slab' geometry, with the slab positioned in the negative x-axis, as illustrated in figure 1. Profiles are normalized to the area under the corresponding curve. Details of each profile comparison are presented in table 2. This table includes a description of the inhomogeneity, its location within the water tank, the measurement/scoring plane position, as well as the average and maximum differences between measurement and calculations, and the 1σ Monte Carlo statistical uncertainty.

Figure 5 illustrates the relative profile dose versus position for 10 MeV electrons incident on the 2 cm thick bone-equivalent half-slab positioned at depths of 0.5 cm and 1.5 cm below the water surface. A significant reduction in the dose is noted directly under the bone-equivalent slab due to attenuation of the electron beam; this dose reduction increases with depth in the

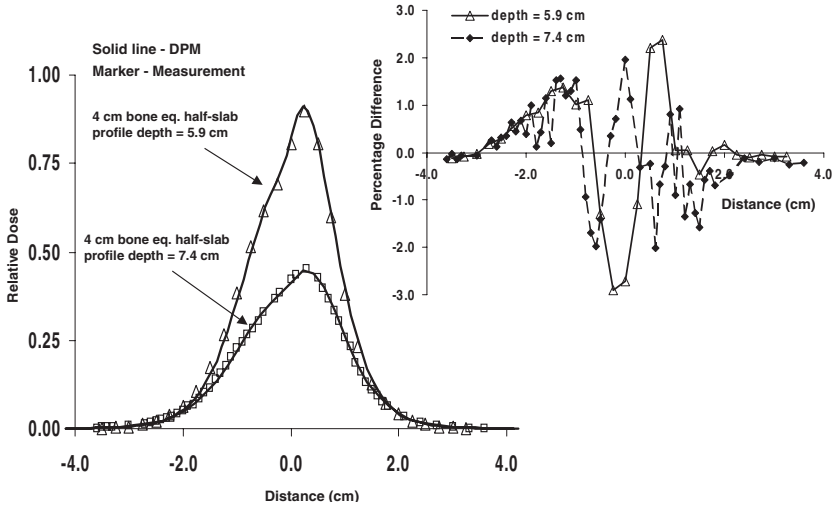

Figure 6. Relative x-axis profile dose for 50 MeV electrons incident on a 4 cm bone-equivalent half-slab positioned at depths of 1.5 cm and 3.0 cm below the water surface. Details of the geometric set-up are provided in table 2. Measurements are shown in the marker and DPM in the solid line. Profiles are normalized to the area under the corresponding curve. The profile for the slab positioned at 3.0 cm depth below the water surface includes a scaling factor of 0.5 for ease of illustration. DPM calculated points represent the centre of voxel values. The 1σ Monte Carlo uncertainty averaged over all calculation points is 1.8% for the slab located at 1.5 cm depth, and 1.2% for the slab at 3 cm depth below the water surface. Shown in the inset are the per cent differences between calculations and measurements for respective profiles. Average and maximum differences between measurements and calculations are provided in table 2. The 1σ Monte Carlo uncertainty ranged from 0.4% in the region of the maximum profile dose to 4.0% in the region less than 10% of maximum dose, for the slab positioned at a depth of 1.5 cm below the water surface. The corresponding 1σ uncertainty range for the slab at a depth of 3.0 cm was 0.8% to 3.2%.

phantom as noted for the profile at greater depth. A shift in the position of the maximum dose from the bone/water interface ($x = 0$) to the water region (positive x-axis) is expected, given the attenuation of the electron beam under bone as well as the scattering of electrons from the higher density bone region to the lower density water region of the interface. The inset of figure 5 illustrates the percentage of differences between measurements and DPM calculations for the respective profiles. Average differences for these comparisons are within $\pm 2\%$; maximum point differences are within $\pm 3.5\%$. Figure 6 shows the relative x-axis profile dose for the 50 MeV electron beam incident on a 4 cm thick bone-equivalent half-slab positioned at depths of 1.5 cm and 3.0 cm below the water surface. There is an expected reduction in the dose under the bone, which is enhanced at greater depths. The loss of electronic equilibrium at the bone/water interface resulting from the scattering of high-energy electrons from the higher density bone to lower density water results in a shift of the maximum dose to the water region of the interface. The per cent differences for the profiles in figure 6 are presented in the inset. Average profile dose differences are 0.8% for the slab positioned at 1.5 cm below the water surface and 1.1% for the slab located at 3 cm below the water surface; respective maximum point differences are -2.9% and 3.3%. The relative profile dose for 10 MeV electrons incident on a 2 cm thick lung-equivalent half-slab situated at depths of 1.5 cm and 3.0 cm below the water surface are presented in figure 7. Both profiles show a considerable reduction in dose under the water region of the interface due to the increased attenuation in water relative to that in the lower density lung material. The inset of figure 7 is a plot of the corresponding

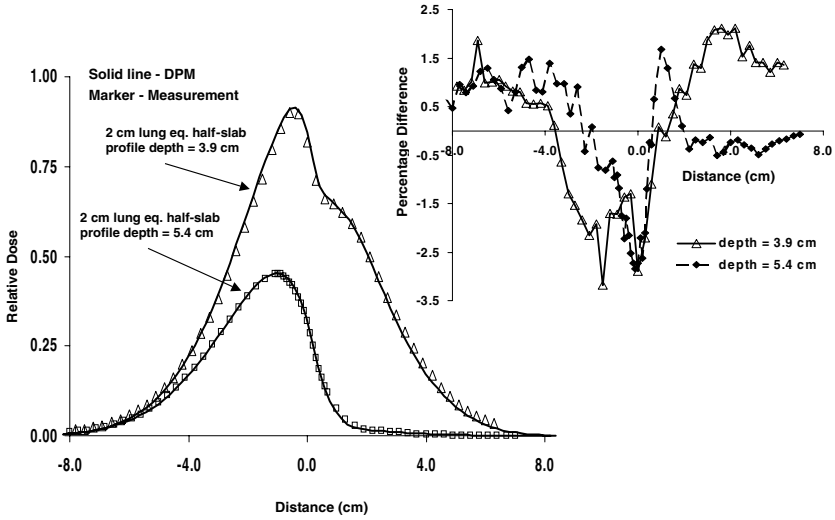

Figure 7. Relative x-axis profile dose for 10 MeV electrons incident on a 2 cm lung-equivalent half-slab positioned at depths of 1.5 cm and 3.0 cm below the water surface. Details of the geometric set-up are provided in table 2. Measurements are shown in the marker and DPM in the solid line. Profiles are normalized to the area under the corresponding curve. The profile for the slab positioned at a depth of 3.0 cm below the water surface includes a scaling factor of 0.5 for ease of illustration. DPM calculated points represent the centre of voxel values. The 1σ Monte Carlo uncertainty averaged over all calculation points is 1.0% for the slab located at a depth of 1.5 cm, and 0.9% for the slab at a depth of 3 cm below the water surface. Per cent differences between calculations and measurements for the corresponding profiles are presented in the inset. Average and maximum differences between measurements and calculations are provided in table 2. The 1σ Monte Carlo uncertainty ranged from 0.4% in the region of the maximum profile dose to 3.0% in the region less than 10% of maximum dose, for the slab positioned at a depth of 1.5 cm below the water surface. The corresponding 1σ uncertainty range for the slab at a depth of 3.0 cm was 0.3% to 2.9%.

profile of percentage differences versus measurement. The average dose difference between the measurements and DPM is 1.3% for the slab located 1.5 cm depth; the maximum difference is -3.2%. Average and maximum profile dose differences for the slab at 3 cm depth are 0.9% and -2.8% respectively. Figure 8 illustrates the relative profile dose for 10 MeV electrons incident on the 4 cm thick lung-equivalent half-slab positioned at depths of 1.5 cm and 3.0 cm below the water surface. The trends noted in these figures are similar to those for the 2 cm lung half-slabs shown in figure 6. There is a reduction in dose under the water region of the profile due to increased attenuation in water as well as scattering of electrons from the lower density lung material into the water region of the interface. The average agreement versus measurements is within $\pm 1.0\%$ (slab at 1.5 cm depth) and 1.1% (slab at 3 cm depth); maximum point differences are within $\pm 3.5\%$ for both these profiles (inset, figure 8).

Figures 5–8 represent a series of profile comparisons conducted using 10 MeV and 50 MeV electron beams incident upon lung- and bone-equivalent half-slabs. Although the average agreement versus measurements are within $\pm 2\%$ for all comparisons, maximum point differences on the order of $\pm 3.5\%$ exist. These differences are likely a combination of measurement uncertainties, as well as systematic uncertainties due to approximations used in determining the electron source particle's angle and energy. A more sophisticated model may be required to correctly account for the angular spread of these electrons, particularly for the 50 MeV beam.

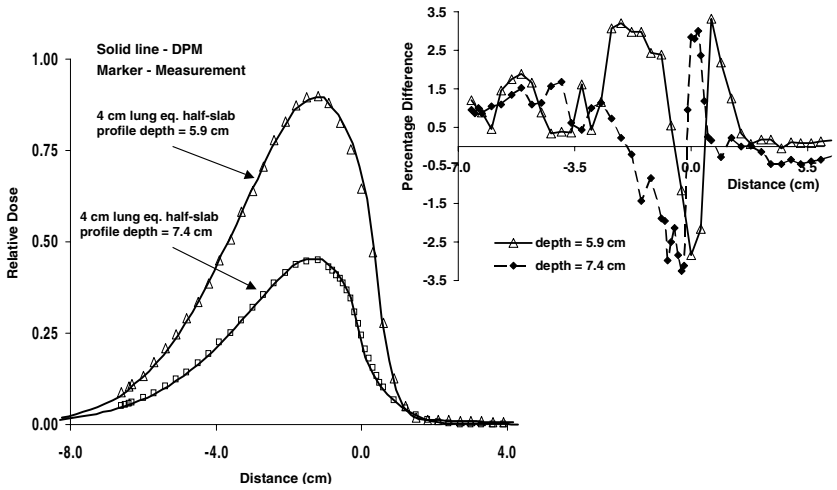

Figure 8. Relative *x*-axis profile dose for 10 MeV electrons incident on a 4 cm lung-equivalent half-slab positioned at depths of 1.5 cm and 3.0 cm below the water surface. Details of the geometric set-up are provided in table 2. Measurements are shown in the marker and DPM in the solid line. Profiles are normalized to the area under the corresponding curve. The profile for the slab positioned at a depth of 3.0 cm below the water surface includes a scaling factor of 0.5 for ease of illustration. DPM calculated points represent the centre of voxel values. The 1σ Monte Carlo uncertainty averaged over all calculation points is 1.0% for the slab located at a depth of 1.5 cm and 1.2% for the slab at a depth of 3 cm below the water surface. Per cent differences between calculations and measurements for respective profiles are illustrated in the inset. Average and maximum differences between measurements and calculations are provided in table 2. The 1σ Monte Carlo uncertainty ranged from 0.5% in the region of the maximum profile dose to 3.5% in the region less than 10% of maximum dose, for the slab positioned at a depth of 1.5 cm below the water surface. The corresponding 1σ uncertainty range for the slab at a depth of 3.0 cm was 0.7% to 3.2%.

Figure 9 shows the profile dose comparison for 50 MeV electrons incident on a 6 cm lung-equivalent half-slab at depths of 1.5 cm and 4.5 cm below the water surface. The large dose enhancement noted beneath the lung region of the interface is predominantly due to the lateral scattering of high-energy electrons from water into lung. Significant differences versus measurements are seen in these profiles; maximum differences of -16.6% and 11.2% are present for the 1.5 cm and 4.5 cm depth slabs respectively (inset, figure 9). It is apparent that the DPM calculations tend to overestimate the dose increase beneath the lung and underestimate the dose below the water region of the interface. For the DPM calculation, the increase in area at the interface region is approximately equal to the reduction in area under the water region of the interface, showing that, in comparison to measurements, DPM calculations predict a significantly greater lateral electron transport at the interface. The reason for this disagreement is not clear at this stage, however, we hypothesize that it is due to the finite size as well as perturbation effects of the ion chamber. Although good agreement was noted for all other profiles, we expect the lateral electron disequilibrium at a lung/water interface to be most severe with 50 MeV, 'pencil-beam' electrons. The reduction in field size associated with the lateral electron transport at the lung/water interface implies that the influence of the ion chamber size on the dose profile will be maximized. We are currently conducting an investigation to model the ion chamber using Monte Carlo methods so as to better understand its effect on the dose profiles. We are also conducting calculations in identical geometries using other Monte Carlo codes, such as MCNP and EGS to ensure that the DPM electron

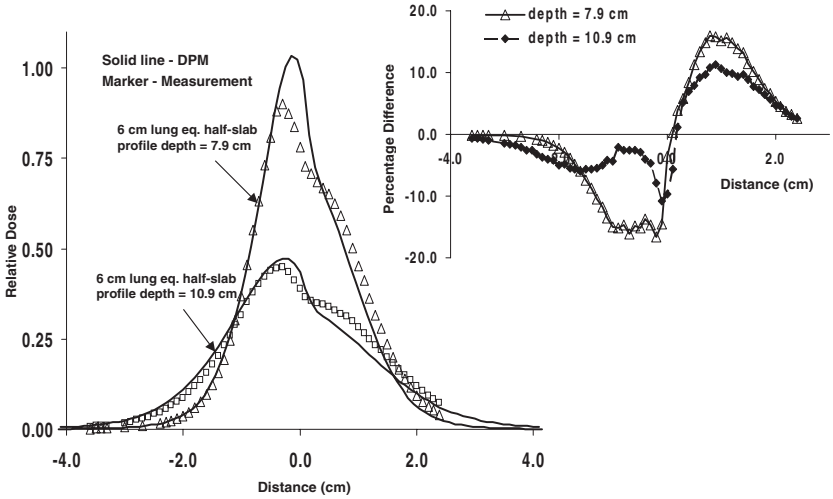

Figure 9. 50 MeV electrons incident on a 6 cm lung-equivalent half-slab positioned at depths of 1.5 cm and 4.5 cm below the water surface. Details of the geometric set-up are provided in table 2. Measurements are shown in the marker and DPM in the solid line. Profiles are normalized to the area under the corresponding curve. The profile for the slab positioned at a depth of 4.5 cm below the water surface includes a scaling factor of 0.5 for ease of illustration. DPM calculated points represent the centre of voxel values. The 1σ Monte Carlo uncertainty averaged over all calculation points is 1.2% for the slab located at a depth of 1.5 cm depth and 1.1% for the slab at a depth of 4.5 cm below the water surface. Per cent differences between calculations and measurements for respective profiles are illustrated in the inset. Average and maximum differences between measurements and calculations are provided in table 2. The 1σ Monte Carlo uncertainty ranged from 0.2% in the region of the maximum profile dose to 4.0% in the region less than 10% of maximum dose, for the slab positioned at a depth of 1.5 cm below the water surface. The corresponding 1σ uncertainty range for the slab at a depth of 3.0 cm was 0.2% to 3.5%.

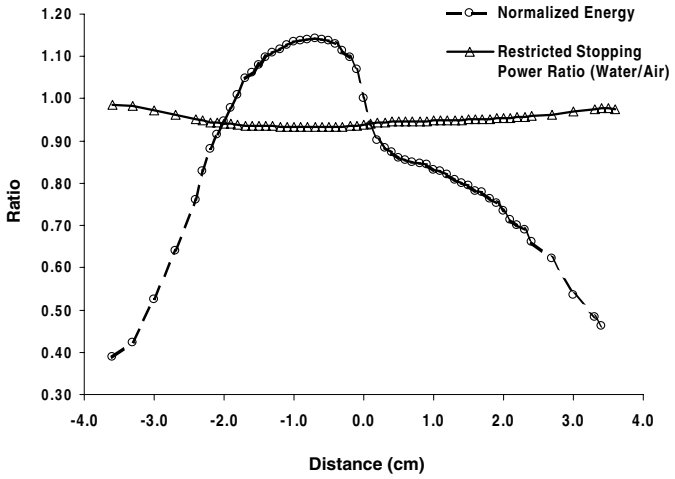

Figure 10. Variation in the mean electron energy and restricted stopping power ratios, $(L/\rho)_{\text{air}}^{\text{water}}$, as a function of position beneath a 6 cm lung-equivalent half-slab, irradiated by 50 MeV electrons. The mean energies were calculated by the Monte Carlo simulation, and represent the average values within the scoring voxels. Shown in the plot are the mean energies normalized to the value at the central axis ($x = 0$). The figure illustrates that although the mean energy varies significantly (by a factor of $\sim$3) across the profile, the stopping power ratios remain relatively constant, with maximum changes on the order of 5%.

transport algorithm, particularly for 50 MeV electrons on lung, is in agreement with these other extensively benchmarked codes. Figure 10 illustrates the variation in normalized mean electron energy and restricted stopping power ratios, $(L/\rho)^{\text{water}}_{\text{air}}$, as a function of the position beneath the 6 cm lung-equivalent half-slab, irradiated by 50 MeV. The mean energies were scored at a depth of 7.9 cm, corresponding to the profile for the slab positioned at 1.5 cm below the water surface (see figure 9). The mean energies have been normalized to the value at the central axis ($x = 0$). It is observed that the mean energies change significantly, by roughly a factor of three across the profile; the energy is increased below the low-density inhomogeneity relative to that below water due to the increased energy loss suffered by electrons in water. Despite the large variation in mean energies across the interface, the stopping power ratios remain relatively constant; the largest variation across the profile is approximately 5%.

4. Conclusion

A series of depth dose and profile ion chamber measurements in both homogeneous and heterogeneous situations has been acquired using minimally scattered electron beams produced from a racetrack microtron. The agreement between DPM and measurements is, on average, well within ±2% for 10 MeV and 50 MeV electrons for the central axis depth dose and profile comparisons in homogeneous-type geometries. Profiles calculated using lung- and bone-equivalent materials to assess the lateral disequilibrium at interface regions are also in good agreement with measurements (on average within ±2%) for all cases except 50 MeV electrons incident on lung. An investigation is currently in progress to evaluate the influence of the ion chamber perturbation on the profile dose in order to explain the large differences (±15%) noted for 50 MeV electrons on lung. We are also conducting a study to validate DPM photon beam calculations in heterogeneous media with the ultimate goal of using DPM for clinical radiotherapy treatment planning.

Acknowledgments

This work has been supported in part by NIH Grant P01-CA59827. The authors are indebted to Dr Pedro Andreo of the Karolinska Institute (Stockholm, Sweden) for his insightful and thoughtful comments, which have undoubtedly helped to strengthen this paper. We would like to thank Lianyan Liu and Shigeru Yokoyama for their valuable help with this project. We would also like to thank Anders Larsson of Scanditronix, Uppsala, Sweden, for providing details on the treatment head design of the racetrack microtron. One of the authors (AFB) gratefully acknowledges the support of ADAC laboratories, Milpitas, CA, for DPM development.

References

Berger M J 1993 *NISTIR 4999* National Institute of Standards and Technology, Gaithersburg, MD

Brahme A, Kraepelien T and Svensson H 1980 Electron and photon beams from a 50 MeV racetrack microtron *Acta Radiol. Oncol.* **19** 305–19

Briesmeister J F 2000 MCNP^{TM} —a general Monte Carlo *N*-Particle transport code *Los Alamos National Laboratory Report LA-12625-M*

Chetty I J, Moran J M, McShan D L, Fraass B A, Wilderman S J and Bielajew A F 2002 Benchmarking of the DPM Monte Carlo code using electron beams from a racetrack microtron *Med. Phys.* **29** at press

DeMarco J J, Solberg T D and Smathers J B 1998 A CT-based Monte Carlo dosimetry tool for radiotherapy treatment planning and analysis *Med. Phys.* **25** 1–11

Fix M K, Stampanoni M, Manser P, Born E J, Mini R and Ruegsegger P 2001 A multiple source model for 6 MV photon beam dose calculations *Phys. Med. Biol.* **46** 1407–28

Gudowska I, Gudowski W, Andreo P, Brahme A and Kierkegaard J 1999 Calculations of absorbed dose and biological effectiveness from photonuclear reactions in a bremsstrahlung beam of 50 MeV *Phys. Med. Biol.* **44** 2099–125

Karlsson M, Nystrom H and Svensson H 1992 Electron beam characteristics of the 50-MeV racetrack microtron *Med. Phys.* **19** 307–15

Kawrakow I and Fippel M 2000 Investigation of variance reduction techniques for Monte Carlo photon dose calculation using XVMC *Phys. Med. Biol.* **45** 2163–83

Keall P J, Siebers J V, Arnfield M, Kim J O and Mohan R 2001 Monte Carlo dose calculations for dynamic IMRT treatments *Phys. Med. Biol.* **46** 929–41

Liu S, Andreo P, Satherberg A, Gudowska I and Brahme A 1995 Monte Carlo simulation of therapy accelerators: application to a 50 MeV racetrack microtron *Radiother. Oncol.* **37** (Suppl 1) 119

Lovelock D M J, Chui C S and Mohan R 1995 A Monte Carlo model of photon beams used in radiation therapy *Med. Phys.* **22** 1387–94

Ma C M, Kapur A, Pawlicki T, Findley D, Brain S and Forster K 1999 Clinical implementation of a Monte Carlo treatment planning system *Med. Phys.* **26** 2133–43

Ma C M, Kapur A, Pawlicki T, Jiang S B and Deng J 2000 *Proc. 13th Int. Conf. on the use of Computers in Radiation Therapy* ed W Schlegel and T Bortfeld, pp 123–25

Rogers D W O, Faddegon D A, Ding G X, Ma C M, We J and Mackie T R 1995 BEAM: A Monte Carlo code to simulate radiotherapy treatment units *Med. Phys.* **22** 503–24

Schach von Wittenau A E, Cox L J, Bergstrom P M, Chandler W P and Hartmann-Siantar C 1999 Correlated histogram representation of Monte Carlo derived medical accelerator photon output phase space *Med. Phys.* **26** 1196–211

Sempau J, Sánchez-Reyes A, Salvat F, Oulad ben Tahar H, Jiang S B and Mackie T R 2001 Monte Carlo simulation of electron beams from an accelerator head using PENELOPE *Phys. Med. Biol.* **46** 1163–86

Sempau J, Wilderman S J and Bielajew A F 2000 DPM, a fast, accurate Monte Carlo code optimized for photon and electron radiotherapy treatment planning dose calculations *Phys. Med. Biol.* **45** 2263–91

Wang L, Chui C S, Kapur A and Lovelock M 1998 A patient-specific Monte Carlo dose-calculation method for photon beams *Med. Phys.* **25** 867–78